electronic supplementary information for

Electronic structure of ultra-thin tellurium nanoribbons †

Zhaofeng Liang[abc], Yao Wang[d], Chenqiang Hua[a], Chengcheng Xiao[e], Miaogen Chen[f], Zheng Jiang[bc], Renzhong Tai[bc], Yunhao Lu[*ae] and Fei Song[*bc]

[a] Department of Physics, Zhejiang University, Hangzhou, 310027, P. R. China.

E-mail:luyh@zju.edu.cn

[b] Shanghai Synchrotron Radiation Facility, Zhangjiang Laboratory, Chinese Academy of Sciences, Shanghai, 201204, P. R. China.

E-mail: songfei@sinap.ac.cn

[c] University of Chinese Academy of Sciences, Beijing, 100100, P. R. China.

[d] College of Materials Science and Engineering, Zhejiang University of Technology, Hangzhou, 310014, P. R. China.

[e] State Key Laboratory of Silicon Materials, School of Materials Science and Engineering, Zhejiang University, Hangzhou, 310027, P. R. China.

[f] Department of Physics, China Jiliang University, Hangzhou, 310018, P. R. China.

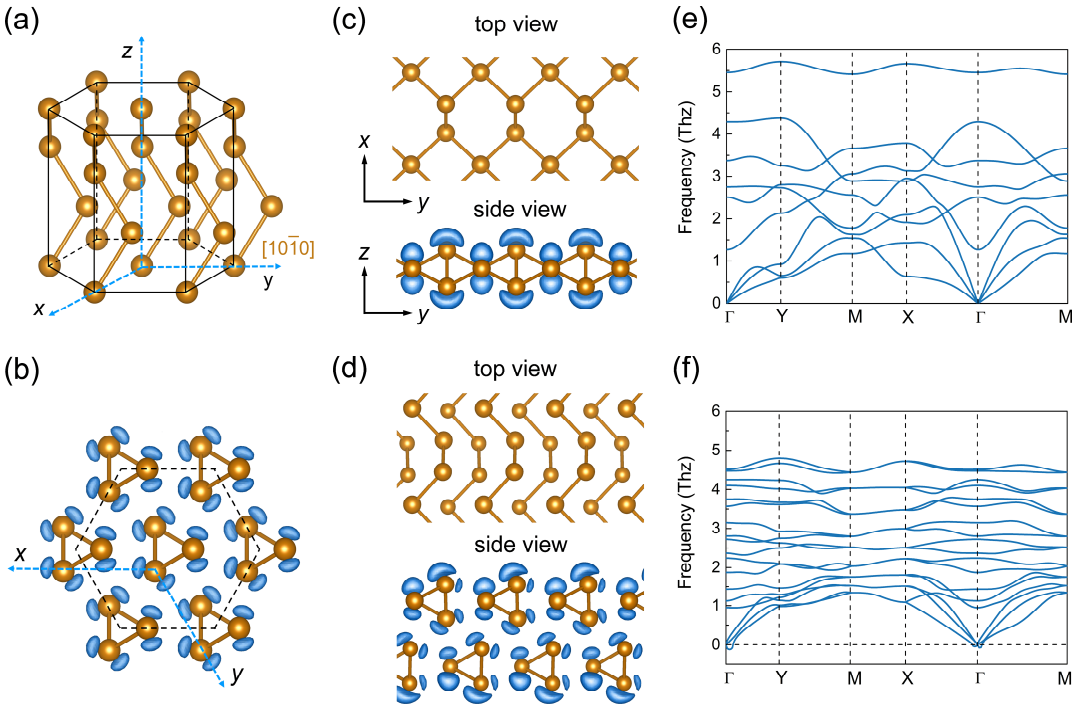

Fig. S1 The stable geometric structures of Te allotropes. (a-b) The structure of bulk α-Te phase and its top view. (c-d) Top and side view for the monolayer (ML) β-Te phase and bilayer (BL) α-Te phase. Visualization of electron localization function (ELF) is also plotted in (b-d), with blue isosurfaces in units of e/Bohr^3, respectively, which characterizes the lone pairs. (e-f) Phonon spectra for the ML β-Te phase and BL α-Te phase (cited from the reference of *Materials Horizons, 2018, 5, 521-528*).

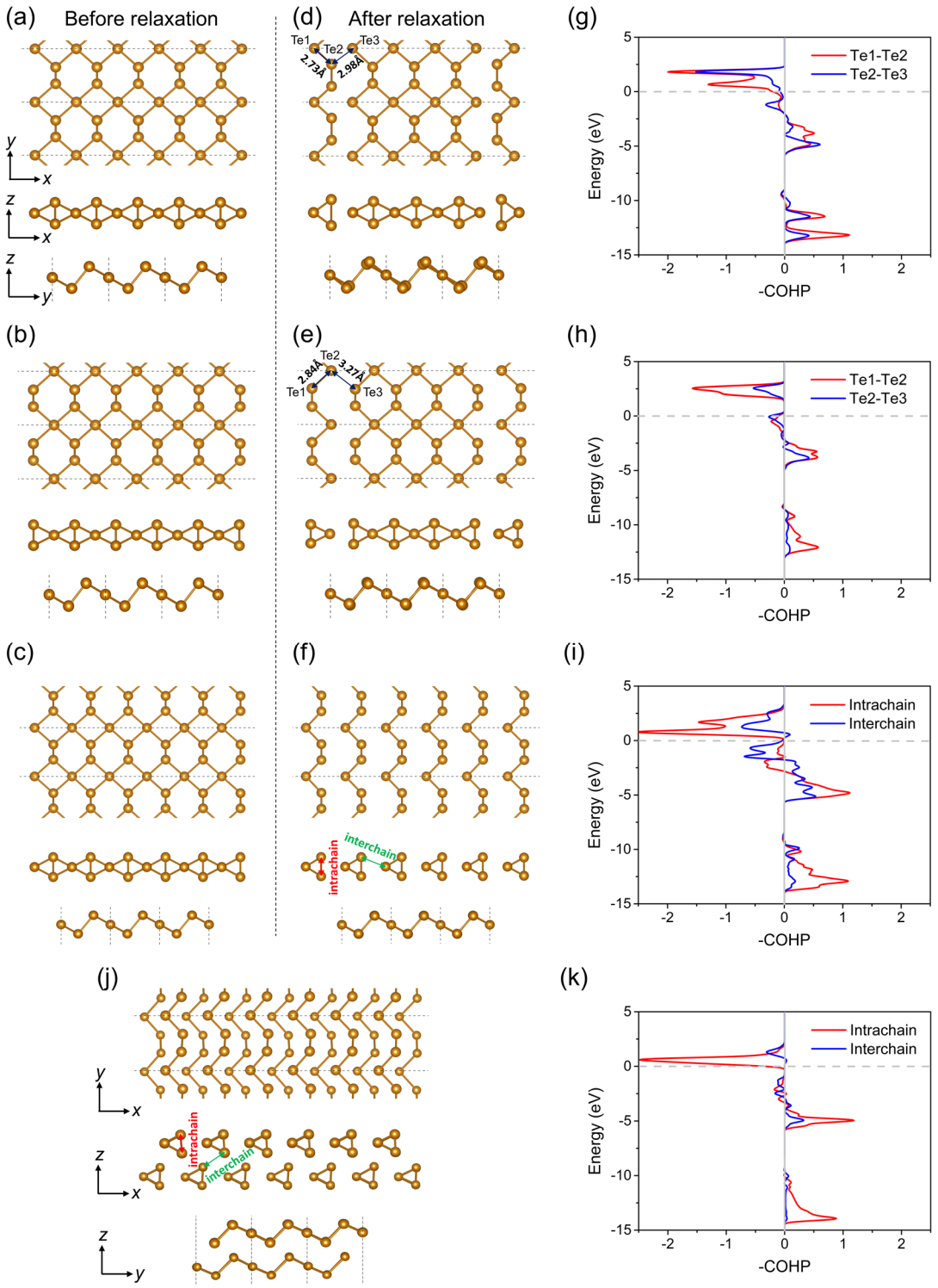

Fig. S2 The geometric structures of ML 6-t-TNR, 6-n-TNR and 6-c-TNR before (a-c) and after (d-f) geometry optimization, respectively. (g-i) COHP for Te bonds in the ML geometry-optimization structures of 6-t-TNR, 6-n-TNR and 6-c-TNR, where Te1-Te2 and Te2-Te3 in both 6-t-TNR and 6-n-TNR represent the edge and edge-interior Te-Te bonds respectively. (j) The geometry-optimization structure of BL 13-c-TNR, and its corresponding COHP (k) for intra- and interchain Te bonds. The positive and negative COHP values represent Te-Te bonding and antibonding character.

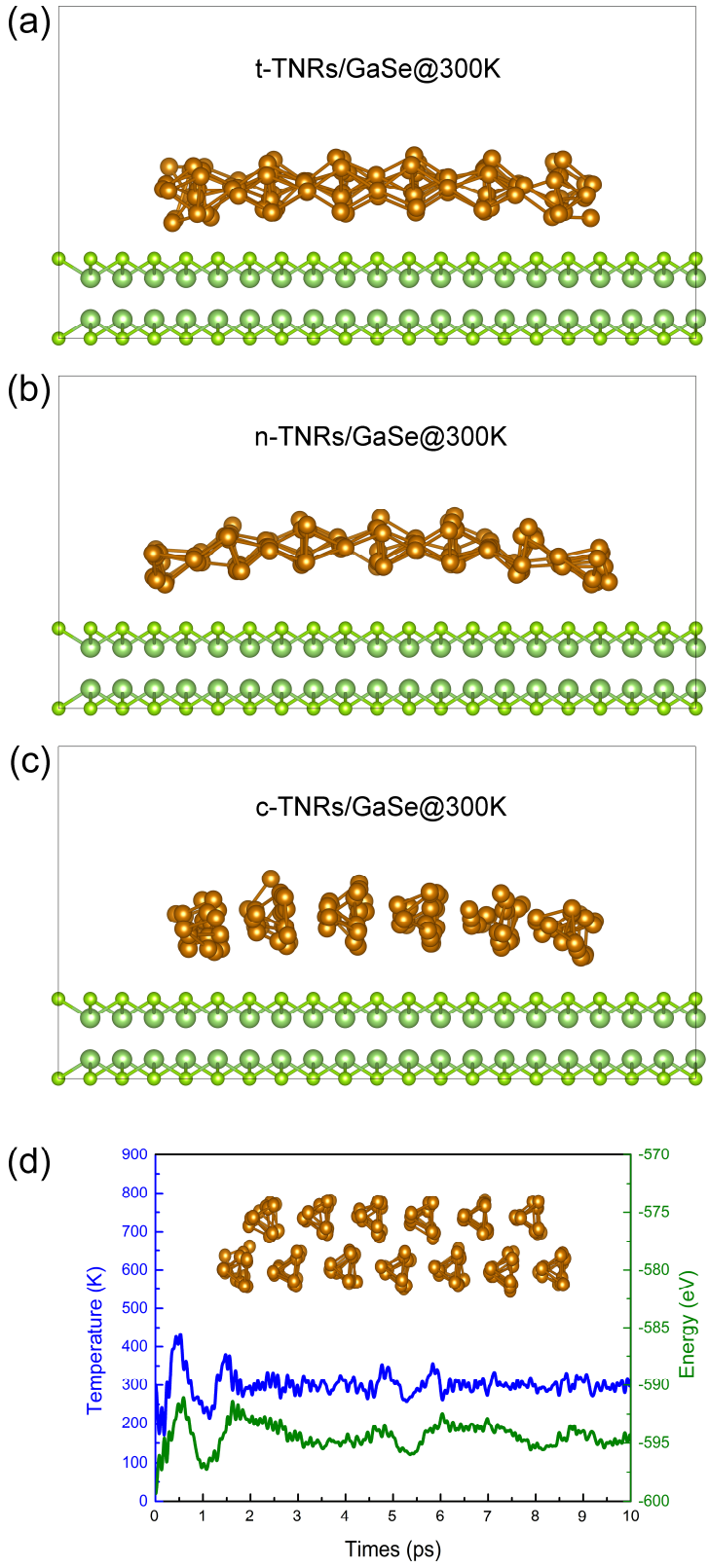

Fig. S3 Ab initio molecular dynamics (AIMD) simulation of TNRs. The structural snapshots (side view) of ML (a) t-TNRs (b) n-TNRs and (c) c-TNRs on GaSe surface at time of 1 ps during AIMD simulation under the temperatures of 300K, respectively. (d) Energy and temperature fluctuation with respect to the time for BL 13-c-TNR. The insert is the structural snapshot (side view) of BL 13-c-TNR at time of 10 ps during AIMD simulation under the temperatures of 300 K.

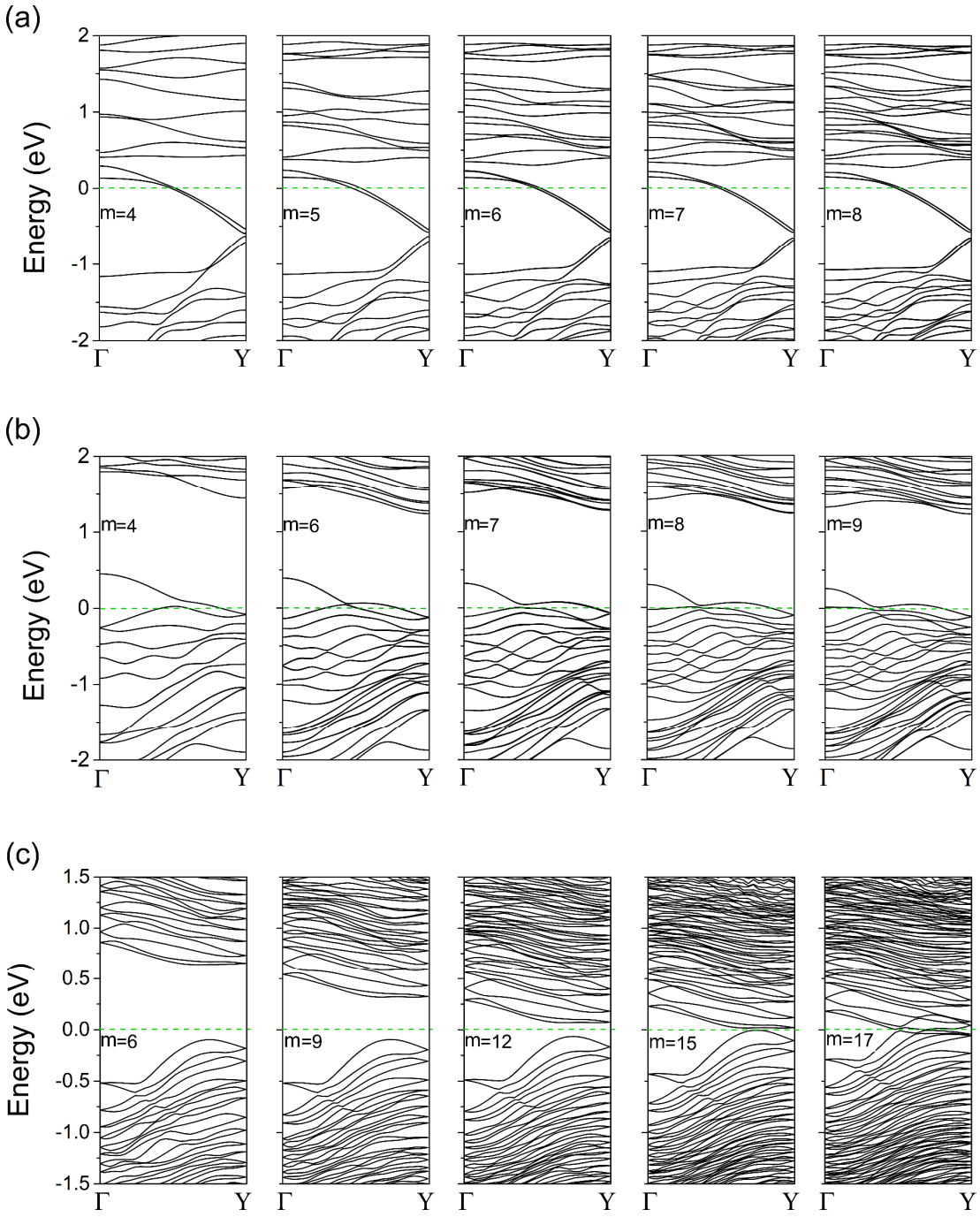

Fig. S4 The band structures of (a) ML t-TNRs, (b) ML n-TNRs and (c) BL c-TNRs with various widths (m). The Fermi level is set to zero and marked by green dashed line.

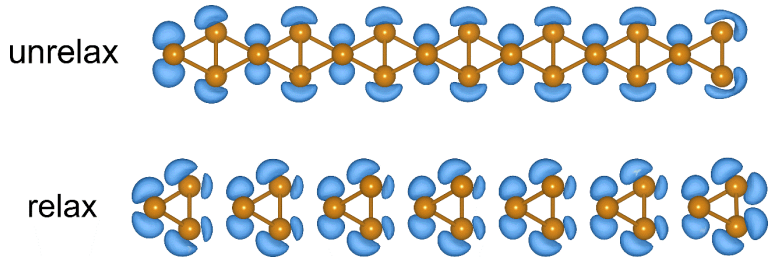

Fig. S5 The unrelaxed and relaxed structure of ML 7-c-TNR, with the visualization of ELF (plotted with blue isosurfaces in units of e/Bohr^3). For the unrelaxed case, the charge distribution at the two asymmetric edges is inconsistent, driving the emergence of chain structure (after relaxation), which exhibits saturated bonding character and helps to maintain the structural stability.

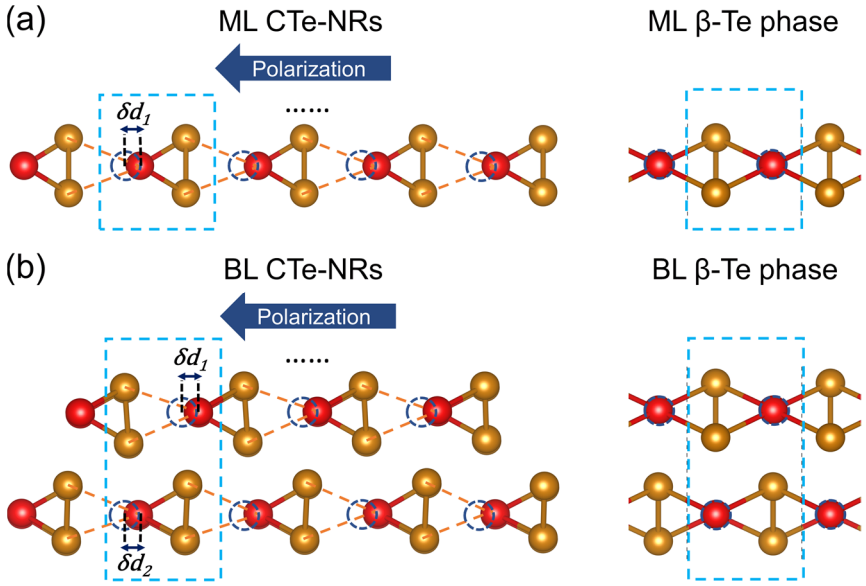

Fig. S6 Side views of the distorted structures of both (a) ML and (b) BL c-TNRs (left), and undistorted centrosymmetric structures of (a) ML and (b) BL β-Te phase (right) which are indicated as reference. Shift of the layer-central Te atoms (red colored) is indicated by mazarine dash circles, and the corresponding displacement is depicted as δd_i. The rectangle with blue dashed lines indicates the unit cell. Therefore, this 2D in-plane polarization model within the Born effective charge theory can be defined as:

$$P_s = \frac{e}{S}\sum_{i}^{N} Z_i^* \, \delta d_i$$

where P_s is the spontaneous electronic polarization, e is the elemental charge, S is the unit cell's area, Z_i^* represents the Born effective charge of the Te in the unit cell. Particularly, for BL c-TNRs, the charge transfer at the inter-layer are neglected herein.

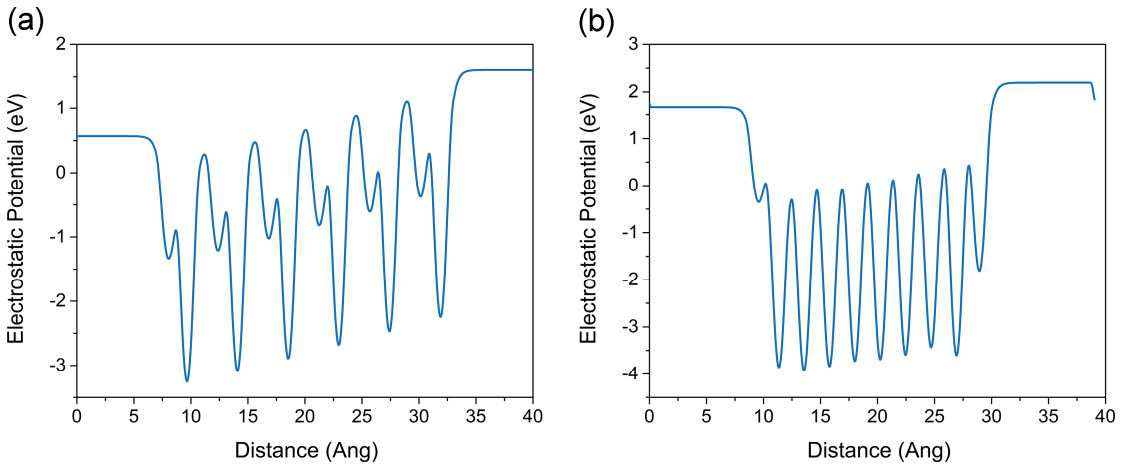

Fig. S7 The average electrostatic potential along the x direction for (a) ML 6-c-TNR and (b) BL 9-c-TNR, respectively. The electrostatic potentials are not equivalent on both edges and there is a gradient from one side to the other, indicating in-plane electronic polarization across the ribbon.

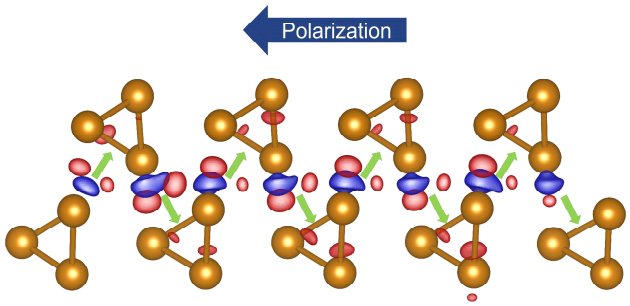

Fig. S8 The profile of charge density difference at the inter-layer of BL 9-c-TNR, defined as $\Delta\rho=\rho-\rho_{top\text{-}Te}-\rho_{bottom\text{-}Te}$, where ρ is the total charge density of the whole ribbon, $\rho_{top\text{-}Te}$ and $\rho_{bottom\text{-}Te}$ are the charge density of the top layer and the bottom layer Te atoms, respectively. The charge accumulation (depletion) region is represented by red (purple) color. The electric dipoles and directions of inter-layer Te chains are shown by the green arrows.

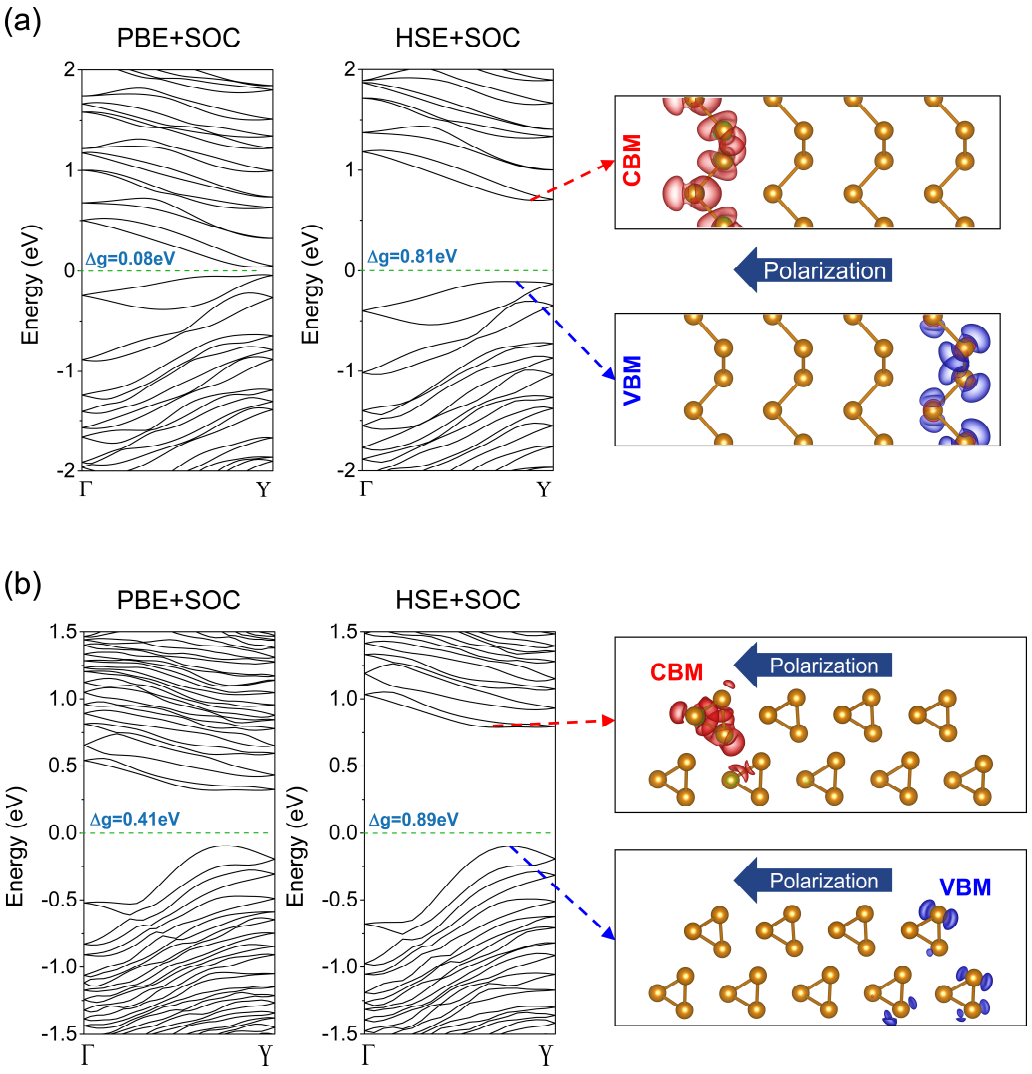

Fig. S9 Band structures of (a) SL 4-c-TNR and (b) BL 9-c-TNR obtained by Perdew-Burke-Ernzerhof-spin-orbit coupling (PBE+SOC) and Heyd-Scuseria-Ernzerhof (HSE+SOC) functionals. The corresponding spatial distribution of wave functions for the VBM and CBM (HSE+SOC) are plotted with red and purple color, respectively. Δg represents the value of band gap. The Fermi level is set to zero and marked by green dashed line.